



A Journal of



Accepted Article

Title: Dual functional half-sandwich Ru(II) complexes: lysosome-targeting probes and anticancer agents

Authors: Zhe Liu, JuanJuan Li, Deliang Kong, Meng Tian, Yao Zhao, Zhishan Xu, Wenyuan Gao, and Yumin Zhou

This manuscript has been accepted after peer review and appears as an Accepted Article online prior to editing, proofing, and formal publication of the final Version of Record (VoR). This work is currently citable by using the Digital Object Identifier (DOI) given below. The VoR will be published online in Early View as soon as possible and may be different to this Accepted Article as a result of editing. Readers should obtain the VoR from the journal website shown below when it is published to ensure accuracy of information. The authors are responsible for the content of this Accepted Article.

To be cited as: *Eur. J. Inorg. Chem.* 10.1002/ejic.201801339

Link to VoR: <http://dx.doi.org/10.1002/ejic.201801339>

WILEY-VCH

Dual functional half-sandwich Ru(II) complexes: lysosome-targeting probes and anticancer agents

Zhe Liu,^{[a]‡*} JuanJuan Li,^{[a]‡} Deliang Kong,^[a] Meng Tian,^[a] Yao Zhao,^[b] Zhishan Xu,^[a,c] Wenyan Gao,^[a] Yumin Zhou.^[a]

^[a] Institute of Anticancer Agents Development and Theranostic Application, The Key Laboratory of Life-Organic Analysis and Key Laboratory of Pharmaceutical Intermediates and Analysis of Natural Medicine, Department of Chemistry and Chemical Engineering, Qufu Normal University, Qufu 273165, China.

^[b] CAS Key Laboratory of Analytical Chemistry for Living Biosystems, Institute of Chemistry, Chinese Academy of Sciences, Beijing 100190, PR China

^[c] Department of Chemistry and Chemical Engineering, Shandong Normal University, Jinan 250014, China.

[‡]The first two authors are equal first authors.

Abstract

It is known that the proposed biologically active form of ruthenium is its oxidation state II other than oxidation state III, and Ruthenium complexes offer the potential of a novel mechanism of action, reduced toxicity. Herein, three half-sandwich Ru^{II} complexes $[(\eta^6-p\text{-cym})\text{Ru}(\text{N}^{\wedge}\text{N})\text{Cl}]\text{PF}_6$ were designed and synthesized. Lysosomes are involved in various aspects of cancer cell immortalization and cell death. Thus, lysosomes are attractive pharmacological targets for selective killing of cancer cells. We demonstrated that **Ru2** can accumulate in lysosomes. In addition, A549 cell variability remained at 87.81% after exposure to **Ru2** for 24 h at the working concentration. Meanwhile, **Ru2** exhibited relatively high photostability and suitability for long-term tracking. At increased concentration after 24 h of exposure to the complex toward A549 cell line, **Ru2** induced a high apoptotic rate, cell cycle arrest, mitochondrial membrane potential loss, and reactive oxygen species overload. **Ru2** integrated the anticancer properties and imaging capabilities and is expected to be developed as a dual functional theranostic agent.

Keywords. Anticancer agents; Apoptosis; Lysosome-targeting probes; Photostability; Ruthenium.

Introduction

Transition metal complexes remain a significant resource to produce chemical diversity in the search for new diagnostic and therapeutic agents,¹⁻⁵ for a relatively readily subtle or dramatic change of the characteristics of the complex by alter-related ligands. Therefore, biological applications of transition metal complexes have been greatly explored, especially in the anticancer drug development.⁶⁻¹⁴ Cisplatin (CDDP), oxaliplatin (OXA), and carboplatin represent the most active and useful clinical transition metal anticancer agents, approximately nearly 50% of all anticancer therapies globally. These drugs are especially effective in treating lung and ovarian cancer. These successes demonstrated that utilization of metals in medicine may be a useful strategy in drug design and development. However, similar to other cytotoxic drugs, problems of platinum-based anticancer drugs, normal tissue toxicity, and drug resistance limit their future use.¹⁵ These factors necessitate the exploration of new chemotype anticancer agents that have metal and new mechanisms of action different from platinum.¹⁶⁻²⁰

Very recently, ruthenium (Ru) complexes have been reported to possess great potential in the search for therapeutic agents. These agents not only showed rich redox chemistry (Ru^{II} and Ru^{III}) but also had less toxicity than their platinum analogs.²¹ Recent study by Dyson has shown that ruthenium arene complexes containing α -diimine ligands have appeared as potential anticancer agents.²² Previous investigators have demonstrated that ruthenium compounds have displayed potent anticancer activities,²³⁻²⁵ such as three ruthenium complexes (NAMI-A, KP1019, and KP1339) and have entered clinical trials.^{21,26} In contrast to the nuclear targets, Ru anticancer drug (e.g., NAMI-A) is one of the mitochondrion and cell surface target agents, indicating that the mitochondrion, the cell surface, and other organelles targets have also been implicated in the anticancer activity of Ru complexes.²⁷⁻³² In this regard, we are interested in the synthesis of novel Ru (II) organometallic arene complexes based on N[^]N-chelating ligands. We also investigated the effects of N[^]N-chelating ligands on the chemical and biological activities. N[^]N-chelating ligand derivatives with different substitution patterns have recently drawn attention as promising catalyst for polymerization. Incorporation of the electron withdrawing groups into the imino ligands can also enhance both the catalytic activity and selectivity of the complex.³³ In addition to promising catalytic activity, N[^]N-chelating ligand derivatives provide the prospect for structural diversification through metal complexation.

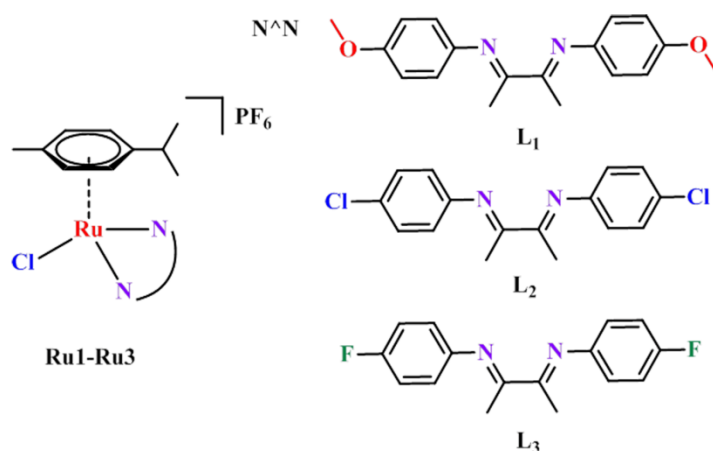
In this study, we choose the diimino as N[^]N-chelating ligands to construct half-sandwich Ru^{II} complexes $[(\eta^6\text{-}p\text{-cym})\text{Ru}(\text{N}^{\wedge}\text{N})\text{Cl}]\text{PF}_6$, **Ru1**, **Ru2**, and **Ru3**, (**Scheme 1**) as theranostic agents. We explored the cell toxicity, photobleaching and the mechanism of action (MOA) of these metal complexes. The study MOA including catalytic hydride transfer analysis, cellular distribution and uptake cell cycle, ROS, and apoptosis. The results suggested that three Ru^{II} complexes are potential candidates for development as new therapeutic agents and long-term lysosome tracking agents.

Results and Discussion.

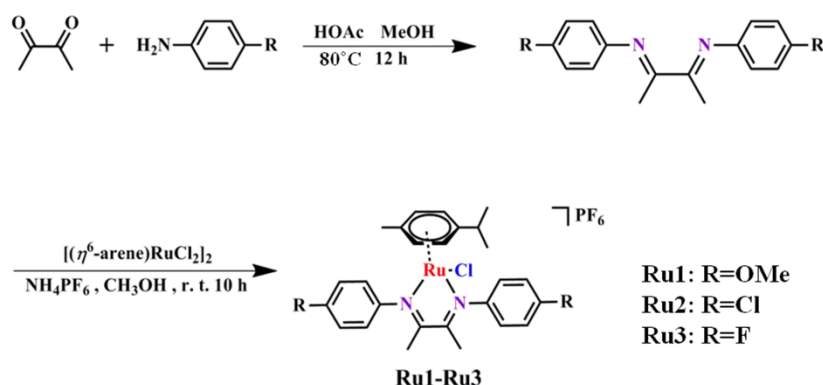
Syntheses.

Dimeric μ -chloro-bridged complex $[(\eta^6\text{-}p\text{-cym})\text{RuCl}_2]_2$ (**dimer**) formed upon conversion of α -terpinene with RuCl₃ under refluxing in absolute methanol.³⁴ The N[^]N-chelating ligand were synthesized by 2,3-butanedione and aniline derivative under the conditions of HOAc (1ml) and MeOH refluxed for 12 h. **Ru1**, **Ru2**, and **Ru3** were synthesized in high yields by stirring at room

temperature the dinuclear ruthenium dimer and the corresponding ligands L₁-L₃ in methanol under N₂ atmosphere and then purified by recrystallization (see Supporting Information and **Scheme 2**). **Ru1**, **Ru2**, and **Ru3** were identified by ¹HNMR, elemental analysis and ESI-MS.



Scheme 1. Chemical Structures of ruthenium(II) complexes



Scheme 2. Synthesis ruthenium (II) arene complexes containing N[^]N ligands.

Photo Physical Properties and Hydrolysis Studies.

At the beginning, we tested the UV–Vis spectra of **Ru1**, **Ru2**, and **Ru3** acquired in phosphate-buffered solutions at 298 K (**Figure S1**). The intense absorption bands of these complexes range at approximately at 250–600 nm. These bands could be assigned to the mixed charge-transfer modes, such as singlet and triplex metal-to-ligand charge transfer (¹MLCT and ³MLCT), mixed ligand-centered transition, and ligand-to-ligand charge transfer.^{28, 35} We tested the hydrolysis of complexes **Ru1**, **Ru2**, and **Ru3** in 10% MeOH/90% H₂O (v/v) by using UV–Vis at 298 K (**Figure S2** in the Supporting information). No clear change was observed over 6 h for those complexes, suggesting that **Ru1**, **Ru2**, and **Ru3** do not hydrolyze at this condition.

Cytotoxicity.

The in vitro cytotoxicity of the organometallic complexes and cisplatin (control) was screened in vitro against HeLa (human cervical cell cancer) and A549 (nonsmall cell lung cancer) cell lines by using MTT assay after 24 h or 72 h treatment. The half-maximal inhibitory concentration (IC₅₀) values are listed in **Table 1** and shown in **Figure S3** in the Supporting Information, wherein

cisplatin was used as the standard control. **Ru1**, **Ru2**, and **Ru3** showed medium anticancer activity against HeLa cell line after 24 h incubation. However, the recorded IC_{50} values of the complexes showed comparable activity toward HeLa cell line after 72 h incubation. These complexes exhibited better anticancer activity against A549 cell line compared with HeLa cell line whether at 24 h or 72 h. For complex **Ru2** (22.2 μ M) equipotent to cisplatin (21.3 μ M) after 24 h, **Ru1** and **Ru3** were of intermediate value against A549 cell line. However, all complexes showed good activity when incubated for 72 h for A549 cell lines. Notably, **Ru2** demonstrated 4.9-fold greater potency after 72 h incubation than that after 24 h incubation in A549 cells and approximately 1.6-fold greater potency than cisplatin. Previous cytotoxicity studies on ruthenium(II) *p*-cymene anticancer complexes show that a marked increase in the cytotoxicity when aspirin and valproic acid was introduced on α -diimine ligands.²² The resulting IC_{50} values showed that substitution of the alterations to the chelating ligand had minimal effect on inhibitory activity in this study. Next, the antiproliferative activities of **Ru2** against BEAS-2B (human bronchial epithelial normal cell) were also evaluated by MTT assay after 72 h incubation, however, no selectivity was observed for the complex between cancer cells versus BEAS-2B normal cell (IC_{50} = 8.0 \pm 0.5 μ M towards BEAS-2B normal cell).

Table 1. Cytotoxicities (IC_{50}) of **Ru1-Ru3** and Cisplatin towards different cell lines.

Complex	IC_{50} (μ M)				
	BEAS-2B		A549		HeLa
	72 h	24 h	72 h	24 h	72 h
Ru1		27.7 \pm 1.0	5.9 \pm 0.4	33.6 \pm 0.8	8.5 \pm 0.2
Ru2	8.0 \pm 0.5	22.2 \pm 0.9	4.5 \pm 0.7	28.9 \pm 1.7	5.8 \pm 0.5
Ru3		34.5 \pm 0.2	7.8 \pm 0.5	37.8 \pm 1.0	9.7 \pm 0.3
Cisplatin		21.3 \pm 1.7	7.2 \pm 1.0	7.5 \pm 0.2	5.5 \pm 0.4

^a Cells were treated with different concentrations of the ruthenium complexes and cisplatin for 24 h or 72 h. Cell viability was determined by the MTT assay, and data were calculated as described in the experimental section. Data are presented as means \pm SD obtained in at least three independent experiments.

Partition Coefficients (log P).

The in vitro antiproliferative activity and cellular uptake levels of metal complexes were consistent with their relative lipophilicity. The log P values determined for **Ru1-Ru3** were from 0.7 to 3.3 (Table 2). To test the log P of the chloride complexes, NaCl (50 mM) was used for hydrolysis inhibition. The anticancer potential and hydrophobicity of the complexes were correlated in this study. **Ru2** displayed higher hydrophobicity and the most antiproliferative activity than **Ru1** and **Ru3**. Similarly, the same trend that the cytotoxicity of the respective complexes tend to correlate with the observed lipophilicity that they provide reported by Dyson.²²

Table 2. Log P Values for **Ru1-Ru3**^a

Complex	log P	
	mean	SD
Ru1	0.36	0.01
Ru2	1.41	0.19
Ru3	0.32	0.09

^a Results are the means of three independent experiments and are expressed as means \pm SDs.

Catalytic oxidation of NADH.

The coupled nicotinamide adenine dinucleotide (NADH) and its oxidized form NAD^+ play crucial roles as the cofactors in a wide range of biological and biocatalyzed processes, such as energy metabolism and cell death.³⁶ Sadler and co-workers reported that the aqua Ir^{III} cyclopentadienyl complexes can accept a hydride from the coenzyme NADH to catalytically convert NADH to NAD^+ and can be linked to ROS production that can induce severe or sustained ROS stress and directly induces cell death.^{37, 38} Therefore, reactions between metal complexes **Ru1**, **Ru2**, and **Ru3** and NADH were investigated. NADH (100 μM) in a solution of 10% MeOH/90% H_2O (v/v) was used as the control to evaluate the catalytic activity of the complexes. Moreover, the catalytic ability of complexes **Ru1**, **Ru2**, and **Ru3** with NADH was monitored under the same test conditions by UV-Vis at 298 K (**Figure 1**, **Figure S4**). The detection principle was based on the UV absorption difference at 339 nm when the conversion of NADH to NAD^+ the absorption at 339 nm decreased. The turnover numbers (TONs) of **Ru1**, **Ru2**, and **Ru3** were calculated, and the results showed that **Ru1** and **Ru2** had similar TONs (**Ru1**:7.1, **Ru2**:7.4) and approximately 2-fold larger than **Ru3**.

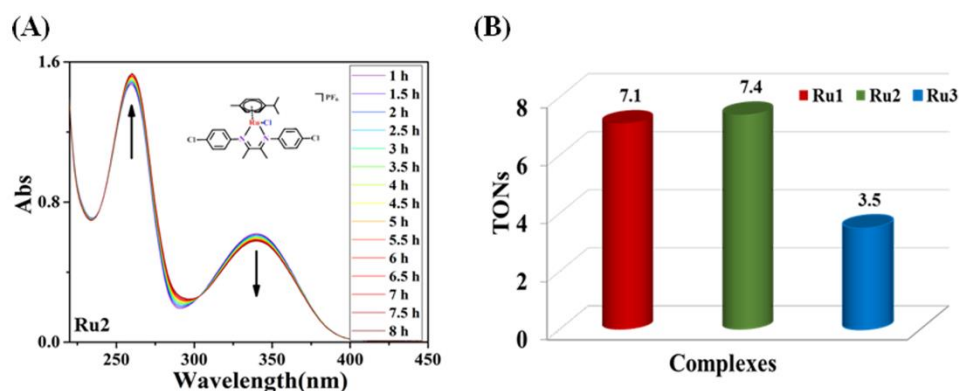


Figure 1. (A) UV-Vis spectra of the reaction of NADH (100 μM) with **Ru2** (1 μM) in 10% MeOH/90 % H_2O (V:V) at 298 K for 8 h; (B) The TONs of as-synthesized complexes. The arrows show changes in absorbance spectra over time.

Cellular Uptake.

Through the above experiments, **Ru2** has high inhibitory activity, hydrophobicity, and catalytic activity. Thus, **Ru2** was selected to carry out further investigations to describe their mechanism of action. Then, we studied the cellular uptake mechanisms of **Ru2**. The cellular uptake mechanisms

include energy-dependent or energy-independent pathways. Energy-dependent pathways can also be divided into active transport and endocytosis. Active transport and endocytosis can be mediated by metabolic inhibitor CCCP and chloroquine (an endocytosis modulator) respectively. Confocal microscopy observations indicated that **Ru2** incubation with A549 cells upon treatment with CCCP or at 4 °C can lead to reduced cellular uptake efficiency (**Figure 2**). However, chloroquine showed no effect on the **Ru2** ability to cross the plasma membrane. The results indicated that **Ru2** entering A549 cells do not rely on the endocytic pathways but possibly through an energy-dependent pathway, e.g., via active transport.

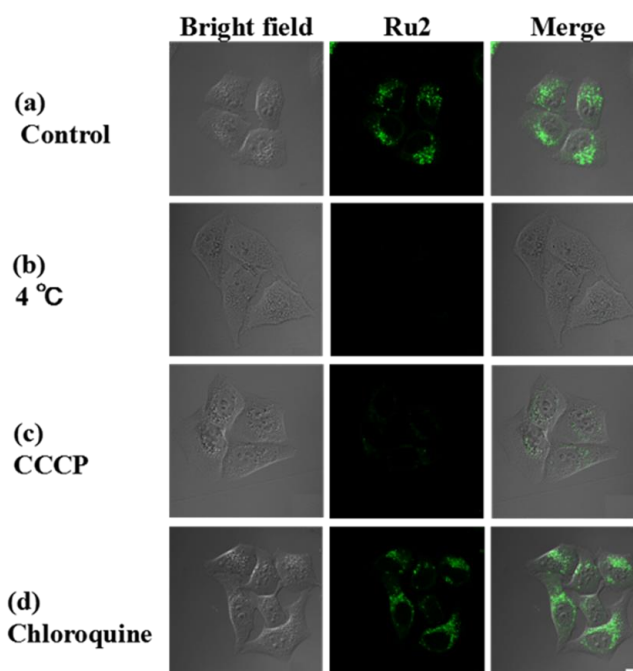


Figure 2. Cellular uptake mechanisms of **Ru2**. Confocal images of A549 cells after incubation with **Ru2** (10 μ M) under different conditions. (a) Cells were incubated with **Ru2** (10 μ M) at 37 °C for 1h. This served as a control. (b) Cells were incubated with **Ru2** (10 μ M) at 4 °C for 1h. (c) Cells were preincubated with metabolic inhibitors CCCP (50 μ M) for 1 h at 37 °C and then incubated with **Ru2** (10 μ M) at 37 °C for 1h. (d) Cells were preincubated with chloroquine (50 μ M) for 1 h at 37 °C and then incubated with **Ru2** (10 μ M) at 37 °C for 1h. Emission was collected at 550 ± 20 nm upon excitation at 488 nm. Scale bars: 10 μ m

Cellular Localization.

The specific cellular target of the complexes determines the initial interactions between cells and complexes and can be observed by confocal microscopy. Considering that lysosomes are involved in various aspects of cancer cell immortalization and cell death, they are emerging as attractive pharmacological targets for selective killing of cancer cells.^{39, 40} The subcellular localization of the complexes was confirmed by confocal microscopy and an inductively coupled plasma mass spectrometry (ICP-MS) assay (**Figure 3**). We probed the specificity of **Ru2** localization with commercial mitochondria staining dye MitoTracker Deep Red (MTDR) and lysosomes staining dye Lyso Tracker Deep Red (LTDR). As shown in **Figures 3A** and **B**, the LTDR signal correlated

well with **Ru2**, providing high Pearson's colocalization coefficient (PCC) at different times (1 h: PCC=0.88, 3 h: PCC=0.90, 8 h: PCC=0.86, and 15h: PCC=0.84). However, minimal overlap is observed for **Ru2** (1 h: PCC=0.06, 3 h: PCC=0.04, and 15 h: PCC=0.07) with MTDR. In the ICP-MS assay, a majority of the **Ru2** localized in the cell membrane after 15 h of co-incubation (**Figure 3C**). In general, lysosomes are a semimembrane vesicular structure of organelles. The results were consistent to the observations of confocal microscopy images. Both of the assays confirmed that **Ru2** can specifically accumulate in the lysosomes for a long-term.

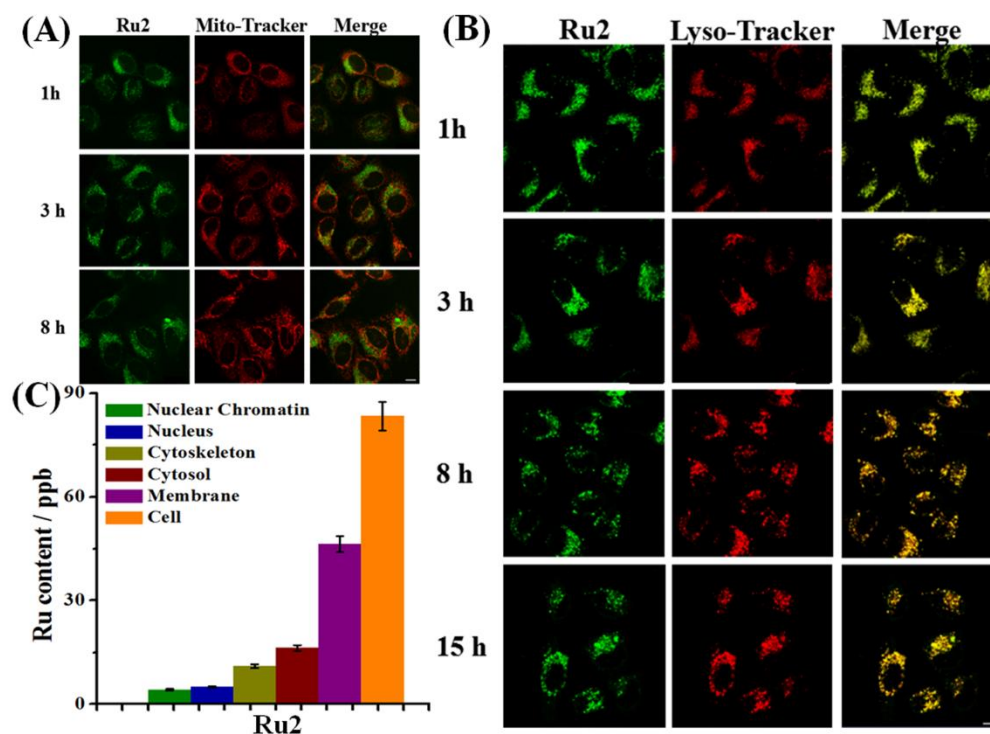


Figure 3. Determination of intercellular localization of **Ru2** by laser confocal microscope. (A) Selective imaging of A549 cells incubated with **Ru2** (10 μ M) for 1 h, 5 h and 8 h; then incubated with MTDR (MitoTracker Deep Red) (75 nM) for 30 min at 37 $^{\circ}$ C. The green and red fluorescence represent **Ru2** and mitochondria, respectively. (B) Selective imaging of A549 cells incubated with **Ru2** (10 μ M) for 1 h, 5 h, 8 h and 15 h; then incubated with LTDR (Lyso Tracker Deep Red) (100 nM) for 30 min at 37 $^{\circ}$ C. The green and red fluorescence represent **Ru2** and the lysosome, respectively. **Ru2**: λ_{ex} = 488 nm; λ_{em} = 550 \pm 20 nm. MTDR: λ_{ex} = 644 nm; λ_{em} = 660 \pm 20 nm. LTDR: λ_{ex} = 594 nm; λ_{em} = 650 \pm 20 nm. Scale bar: 10 μ m. (C) Ruthenium content of the Nuclear Chromatin, Nucleus, Cytoskeleton, Cytosol and Membrane fractions of A549 cells after 24 h of exposure to 10 μ M **Ru2**. Results are the means of two independent experiments in triplicate and are expressed as means \pm SDs.

Apoptosis Assay and Cell Cycle Analysis.

Apoptosis is a common cell death pathway and reported to be the primary pathway for cell death.² To determine the relationship between cytotoxic activity and apoptosis, we treated the lung cancer cells with **Ru2** at 1, 2, and 3 equipotent concentrations of IC_{50} for 24 h and tested by flow cytometry (**Figure 4** and **Table S1** in the Supporting Information). As shown in **Figure 4**, only a

small portion of complex-treated cells (10.89%) are in late apoptosis at $1 \times \text{IC}_{50}$ compared with control (5.22%), and as increased complex concentration the percentage of cells in the apoptotic phase dramatically added. A high apoptotic rate (75.76%) at late apoptotic phase can be achieved for $3 \times \text{IC}_{50}$ of **Ru2** after 24 h co-incubation.

To investigate whether the inhibition of cancer cell proliferation is associated with cell cycle arrest, the cell cycle arrest in A549 cells exposed to **Ru2** was observed using flow cytometry (Figure 4, Table S2 in the Supporting Information). The cell cycle progression was analyzed at 0.25, 0.5, and 1 equipotent concentrations of IC_{50} of **Ru2** for 24 h. The results showed that compared with vehicle treatment, upon exposure of the cells to **Ru2**, a dose-dependent increase in the proportion of G_0/G_1 phase was observed (from 59.63% to 80.02%). The percentages of cells in the G_0/G_1 phase of the cell cycle increased 20.39%. This result demonstrated the complex disturbance of the cell cycle at the G_0/G_1 phase.

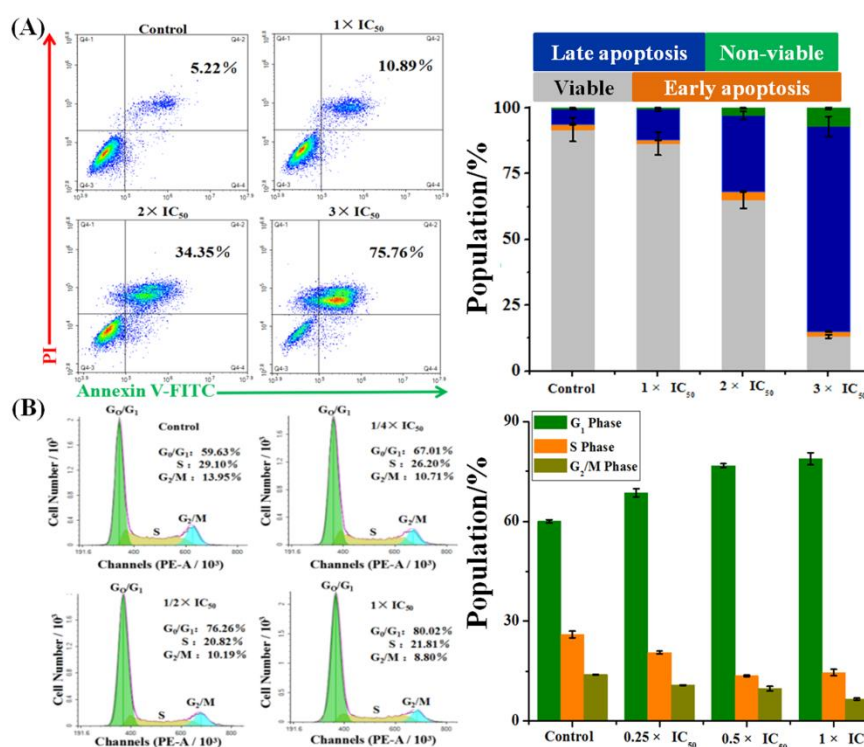


Figure 4. (A) Apoptotic population in A549 cells treated with **Ru2** (1 , 2 , and $3 \times \text{IC}_{50}$) for 24 h. FACS analysis using AnnexinV-FITC/PI. The experiment is repeated three times and representative photographs are displayed. And Columns, mean values of three independent experiments. Data are presented as mean \pm S.D. (B) Effect of **Ru2** (0.25 , 0.5 , and $1 \times \text{IC}_{50}$) on cell cycle of A549 cells by FACS analysis exposed for 24 h. left: FACS analysis. A representative experiment of these three independent experiments is demonstrated. Right: percentage of A549 cells in every phase of cell cycle upon different concentration treatment. The data are expressed as the mean \pm SD from three independent experiments.

Mitochondrial Membrane Potential ($\Delta\psi_m$) Changes and Induction of Intracellular Reactive Oxygen Species (ROS).

The mitochondrion is an essential component of the intrinsic apoptotic signaling pathway. Thus, we further investigated whether complexes induce apoptosis through the mitochondrial damage by

measuring the MMP changes.⁴¹ The MMP loss and the ROS overload are the main pathways in the mitochondria to carry out cell death.^{10, 42} We investigated the intracellular MMP loss and ROS production in **Ru2**-treated A549 cells by using fluorescent probe JC-1 and 2,7-dichlorofluorescein diacetate (DCF-DA) by flow cytometry respectively. Fluorescence change from red to green indicated a decrease in MMP. **Ru2** (at concentrations of 0.25, 0.5, 1, and 2 \times IC₅₀ for 24 h) affects the lost MMP in a dose-dependent manner, as shown in **Figure 5A**. In addition, the percentage of cells with mitochondrial membrane depolarization increased from 6.91% to 73.81% after 24 h treatment. The cause of ROS production was tested using DCF-DA, as shown in **Figure 5B**. A significant increase in a dose-dependent manner was also observed. This finding was consistent with the lost MMP results.

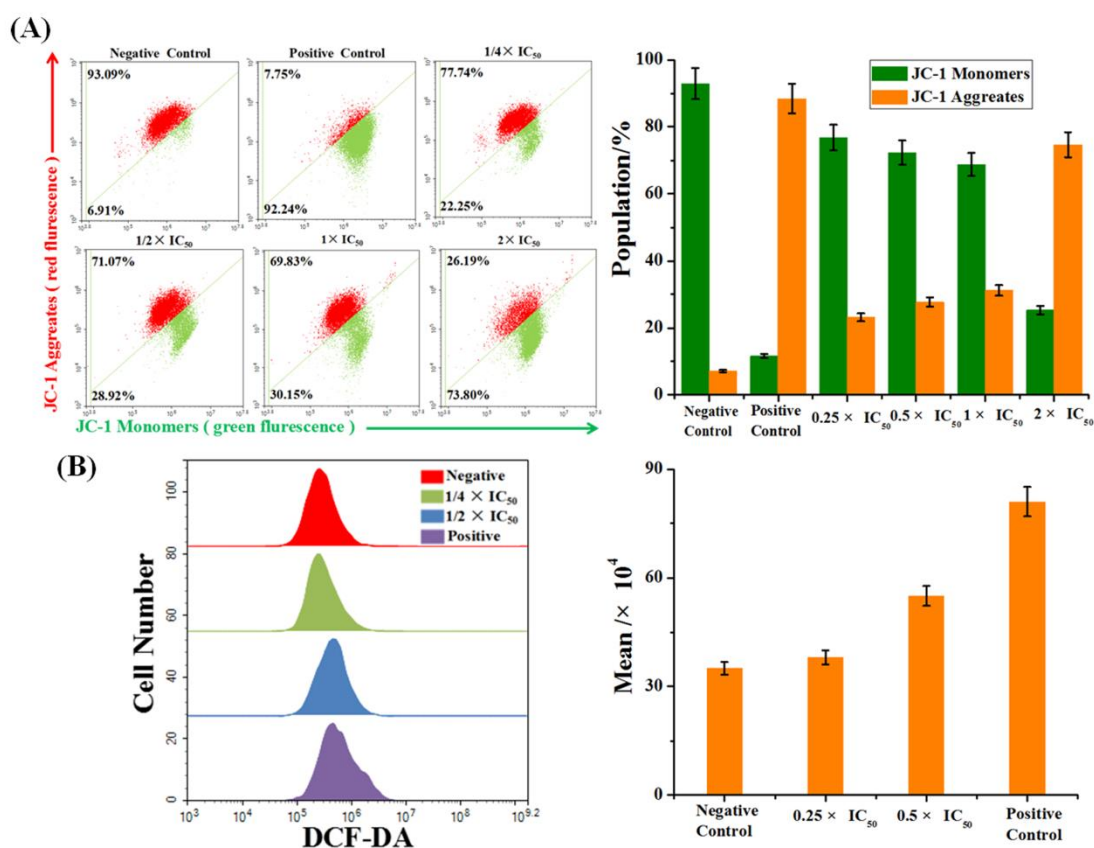


Figure 5. (A) The effect of **Ru2** (0.25, 0.5, 1, and 2 \times IC₅₀) for 24 h on mitochondrial membrane potentials were determined with JC-1 staining by flow cytometry. left: FACS analysis. One representative profile out of three replicates. Right: The bar graph shows the percentage of JC-1 red fluorescence and JC-1 green fluorescence in A549 cells. Each point represents the mean \pm SD of three replicates. (B) Left: Effects of **Ru2** (0.25 and 0.5 \times IC₅₀) for 24 h on ROS levels in A549 cells by flow cytometry. A representative experiment of these three independent experiments was demonstrated. Right: The bar graph shows the mean fluorescence intensity of the generated ROS in A549 cells. Data are presented as mean \pm S.D.

Photobleaching.

The cell variability of **Ru2** at 1 \times IC₅₀ (the working concentration) remains to be 87.81% after

being exposed to A549 cells for 24 h (**Table S1**) and can specifically target lysosomes for a long time (**Figure 3B**). Thus, we explored its potential as a dual-functional theranostic agent. In general, a major shortcoming of a large amount of fluorescent organic bioprobes is its sensitivity to photobleaching. As shown in **Figure 6**, the signal loss percentages after 20 scans were measured to be 56.4% and 75.8% for **Ru2** and LysoTracker Green, respectively. The results indicated that **Ru2** has relatively high cell variability and photostability. This condition is suitable for long-term tracking.

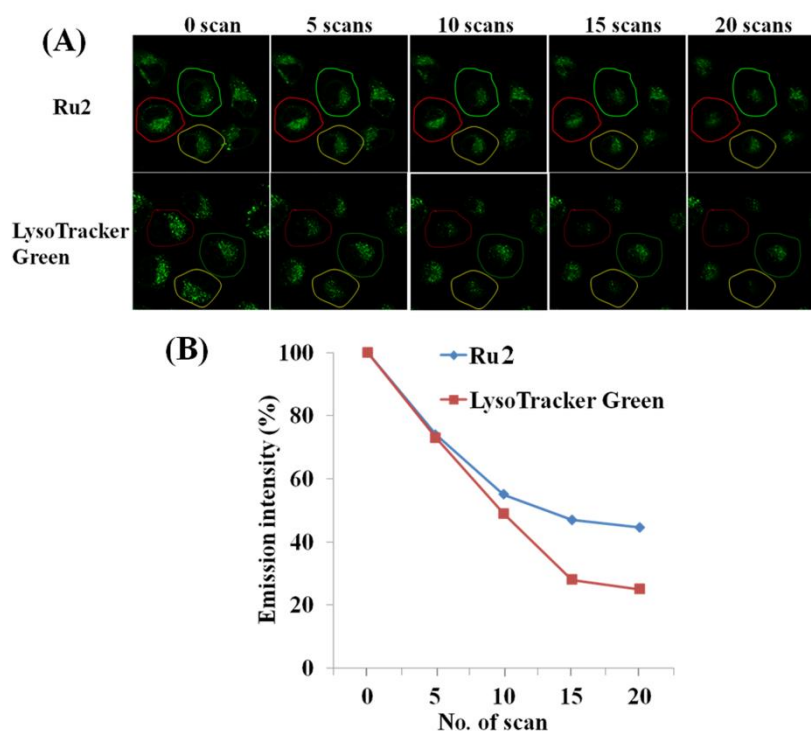


Figure 6. Comparison of photostability between **Ru2** (22.2 μM) and LysoTracker Green (100 nM). (A) Confocal fluorescence images of live A549 cells stained with **Ru2** ($\lambda_{\text{ex}} = 488 \text{ nm}$) or LysoTracker Green ($\lambda_{\text{ex}} = 488 \text{ nm}$) under serial excitation. (B) Luminescence decay curves of **Ru2** and LysoTracker Green after the same serial scans. The signals of **Ru2** and MitoTracker Green were collected at $520 \pm 20 \text{ nm}$.

Conclusion

In summary, three half-sandwich Ru^{II} complexes $[(\eta^6\text{-}p\text{-cym})\text{Ru}(\text{N}^{\wedge}\text{N})\text{Cl}]\text{PF}_6$, namely, **Ru1**, **Ru2**, and **Ru3** as theranostic and specifically lysosomes target agents, were synthesized. **Ru2** is the most potential complex that has high inhibitory activity, higher hydrophobicity and catalytic activity compared with the other two complexes, along with a high apoptotic rate (75.76%), cell cycle arrest, the loss of MMP and the overload of ROS can be achieved for **Ru2** at higher concentration after 24 h. However, cell variability of **Ru2** at $1 \times \text{IC}_{50}$ (22.2 μM , the working concentration) remains to be 87.81% after exposed to A549 cells for 24 h and is suitable for long-term tracking of specific target lysosomes. Meanwhile, **Ru2** had relatively high photostability. The results suggested that these Ru^{II} complexes are potential candidates for development as a dual-functional theranostic agent.

Experimental section

Materials and Instrumentation. Unless otherwise noted, all manipulations were performed using standard Schlenk tube techniques under nitrogen atmosphere. hydrated $\text{RuCl}_3 \cdot n\text{H}_2\text{O}$ ($\geq 99\%$ purity), octan-1-ol ($\geq 99\%$), and Nitric acid (72%), glyoxal, 40 wt.% solution in H_2O , p-toluidine, p-anisidine, 4-fluoroaniline, 4-chloroaniline, 4-methoxyaniline, were purchased from Sigma-Aldrich. Dimer and ligand were prepared as described. For the biological experiments, BSA, carbonyl cyanide m-chlorophenylhydrazone (CCCP), DMEM medium, fetal bovine serum, penicillin/streptomycin mixture, trypsin/EDTA, and phosphate-buffered saline (PBS) were purchased from Sangon Biotech. MTDR (Life Technologies), LTDR (Life Technologies), MTT (3-(4,5-dimethylthiazol-2-yl)-2,5-diphenyltetrazolium bromide, Sigma-Aldrich), Annexin V-FITC Apoptosis Detection Kit (Sigma-Aldrich), JC-1 (Sigma-Aldrich), PBS (Sangon Biotech), PI (Sigma-Aldrich) are all used as received. Testing compounds was dissolved in DMSO and diluted with the tissue culture medium before use.

Syntheses.

Synthesis of the ligands (L_1 - L_3).

Ligands L_1 - L_3 was synthesized according to the literature.

For synthesis of ligand L_1 , a mixture solution of 2,3-butanedione (0.0115 mol), 4-methoxyaniline (0.0235 mol), HOAc (1ml) and MeOH (20 ml) was refluxed for 12 h, after which the resulting suspension was filtered and the solid product washed with MeOH, until the washing phase remained bright yellow and dried in vacuum. Yield: 2.23g 65.5%. ^1H NMR (500 MHz, CDCl_3) δ 6.91 (d, 4H, $J = 7.6$ Hz), 6.78 (d, 4H), 3.84 (s, 6H), 2.17 (s, 6H). Anal. Calcd for $\text{C}_{18}\text{H}_{20}\text{N}_2\text{O}_2$: C, 72.95; H, 6.80; N, 9.45; Found: C 72.90, H 6.85, N 9.42.

For synthesis of ligand L_2 , a process similar to that of L_1 was adopted. 2,3-butanedione (0.023 mol), 4-chloroaniline (0.046 mol) Yield: 6.00g 85.6%. ^1H NMR (500 MHz, CDCl_3) δ 7.175 (d, 4H, $J = 7.6$ Hz), 6.70 (d, 4H, $J = 8.0$ Hz), 2.347 (s, 6H). Anal. Calcd for $\text{C}_{16}\text{H}_{14}\text{Cl}_2\text{N}_2$: C, 62.97; H, 4.62; N, 9.18; Found: C 62.95, H 4.65, N 9.23.

For synthesis of ligand L_3 , a process similar to that of L_1 was adopted. 2,3-butanedione (0.023 mol), 4-fluoroaniline (0.046 mol) Yield: 4.75g 75.9%. ^1H NMR (500 MHz, CDCl_3) δ 7.175 (d, 4H, $J = 7.6$ Hz), 6.70 (d, 4H, $J = 8.0$ Hz), 2.148 (s, 6H). Anal. Calcd for $\text{C}_{16}\text{H}_{14}\text{F}_2\text{N}_2$: C, 70.58; H, 5.18; N, 10.29; Found: C 70.60, H 5.15, N 10.26.

Synthesis of the $[(\eta^6\text{-p-cymene})\text{Ru}(\text{N}^{\wedge}\text{N})\text{Cl}]\text{PF}_6$.

General method: A solution of **dimer** $[(\eta^6\text{-p-cymene})\text{RuCl}_2]_2$ (0.05 mmol) and the corresponding diimine base ligands L_1 - L_3 (0.10mmol) in methanol (20 ml) in a Schlenk bottle was stirring at room temperature in an N_2 atmosphere for 10 h, cool to room temperature. NH_4PF_6 (0.42 mmol) was added after constant stirring 5h. Methanol was removed under reduced pressure, filter and recrystallized from dichloromethane/diethyl ether. The ^1H NMR (500.13 MHz, CDCl_3 or $\text{DMSO-}d_6$) peak integrals of complexes **1**, **2** and **3** are shown as follows.

$[(\eta^6\text{-p-cymene})\text{Ru}(\text{L}_1)\text{Cl}]\text{PF}_6$ (**1**). Yield: 17.3 mg, 48.6%. ^1H NMR (500 MHz, DMSO) δ 7.40 (s, 4H), 7.18 (d, $J = 9.1$ Hz, 4H), 5.14 (d, $J = 6.5$ Hz, 2H), 5.09 (d, $J = 6.4$ Hz, 2H), 3.87 (s, 6H), 2.46 – 2.44 (m, 1H), 2.31 (s, 6H), 2.03 (s, 3H), 1.02 (d, $J = 6.9$ Hz, 6H). ^{13}C NMR (126 MHz, DMSO) δ 177.07 (s), 159.39 (s), 144.54 (s), 88.73 (s), 87.52 (s), 56.02 (s), 30.89 (s), 22.04 (s), 20.60 (s),

18.66 (s). Anal. Calcd for $(\eta^6\text{-p-cymene})\text{Ru}(\text{L}_1)\text{Cl}] \text{PF}_6$ (712.10): C, 47.23; H, 4.81; N, 3.93. Found: C, 47.25; H, 4.86; N, 3.89. MS: m/z 567.14 $[(\eta^6\text{-p-cymene})\text{Ru}(\text{L}_1)\text{Cl}]^+$.

$[(\eta^6\text{-p-cymene})\text{Ru}(\text{L}_2)\text{Cl}]\text{PF}_6$ (**2**). Yield: 14.2. mg, 39.2%. ^1H NMR (500 MHz, DMSO) δ 7.73 (d, $J = 8.8$ Hz, 4H), 7.46 (s, 4H), 5.20 (dd, $J = 22.1, 6.4$ Hz, 4H), 2.32 (s, 6H), 2.03 (s, 3H), 1.03 (d, $J = 6.9$ Hz, 6H). ^{13}C NMR (126 MHz, DMSO) δ 178.08 (s), 149.86 (s), 133.40 (s), 110.14 (s), 103.14 (s), 88.75 (s), 87.13 (s), 30.99 (s), 22.02 (s), 20.76 (s), 18.64 (s). Anal. Calcd for $[(\eta^6\text{-p-cymene})\text{Ru}(\text{L}_1)\text{Cl}]\text{PF}_6$ (722.00): C, 43.32; H, 3.91; N, 3.89. Found: C, 43.36; H, 3.93; N, 3.83. MS: m/z 575.04 $[(\eta^6\text{-p-cymene})\text{Ru}(\text{L}_2)\text{Cl}]^+$.

$[(\eta^6\text{-p-cymene})\text{Ru}(\text{L}_3)\text{Cl}]\text{PF}_6$ (**3**). Yield: 14.7. mg, 42.8%. ^1H NMR (500 MHz, DMSO) δ 7.51 (t, $J = 7.4$ Hz, 8H), 5.19 (dd, $J = 17.4, 6.5$ Hz, 4H), 2.32 (s, 6H), 2.02 (s, 3H), 1.02 (d, $J = 6.9$ Hz, 6H). ^{13}C NMR (126 MHz, DMSO) δ 177.99 (s), 160.82 (s), 147.56 (s), 110.03 (s), 102.69 (s), 88.92 (s), 87.13 (s), 30.92 (s), 21.97 (s), 20.71 (s), 18.56 (s). Anal. Calcd for $[(\eta^6\text{-p-cymene})\text{Ru}(\text{L}_3)\text{Cl}]\text{PF}_6$ (688.06): C, 45.39; H, 4.10; N, 4.07. Found: C, 45.36; H, 4.13; N, 4.10. MS: m/z 543.10 $[(\eta^6\text{-p-cymene})\text{Ru}(\text{L}_3)\text{Cl}]^+$.

NMR Spectroscopy. ^1H NMR spectra were acquired in 5 mm NMR tubes at 298 K on Bruker DPX 500 ($^1\text{H} = 500.13$ MHz) spectrometers. ^1H NMR chemical shifts were internally referenced to $(\text{CHD}_2)(\text{CD}_3)\text{SO}$ (2.50 ppm) for DMSO- d_6 , CDCl_3 (7.26 ppm) (for chloroform- d_1). All data processing was carried out using XWIN-NMR version 3.6 (Bruker UK Ltd.).

UV-Vis Spectroscopy. A TU-1901 UV-Vis recording spectrophotometer was used with 1 cm path-length quartz cuvettes (3 mL). Spectra were processed using UVWinlab software. Experiments were carried out at 298 K unless otherwise stated.

Measurement of Lipophilicity $\text{Log}P_{o/w}$. $\text{log} P_{o/w}$ was calculated as the logarithmic ratio of metal concentration in n-octanol to that in aqueous phase. Octanol-saturated water (OSW) and water-saturated octanol (WSO) were prepared using analytical grade octanol and 50 mM aqueous NaCl solution (to suppress hydrolysis of the chloride complexes). Aliquots of stock solutions of metal complexes in OSW were added to equal volumes of WSO and shaken in an IKA Vibrax VXC basic shaker for 4 h at 500 g/min to allow partition at ambient temperature (~ 298 K). The aqueous layer was carefully separated from the octanol layer for metal complex analysis. Metal was quantified from aliquots taken from the octanol-saturated aqueous samples before and after partition. Partition coefficients of metal complexes were calculated using the equation $\text{log} P = \text{log} ([\text{M}]_{\text{WSO}} / [\text{M}]_{\text{OSW}})$, where $[\text{M}]_{\text{WSO}}$ was obtained by subtraction of the metal content of the aqueous layer after partition from the metal content of the aqueous layer before partition.

Reaction with NADH. The reaction of complex (ca. 1 μM) with NADH (100 μM) in 50% MeOH/50% H_2O (v/v) was monitored by UV-Vis at 298 K after various time intervals. TON was calculated from the difference in NADH concentration after 9 h divided by the concentration of metal complex catalyst. The concentration of NADH was obtained using the extinction coefficient $\epsilon_{339} = 6220 \text{ M}^{-1}\text{cm}^{-1}$.

Cell Culture. A549 cervical carcinoma cells were obtained from Shanghai Institute of Biochemistry and Cell Biology (SIBCB) and were grown in Dubelco's Modified Eagle Medium (DMEM). All media were supplemented with 10% fetal bovine serum, and 1% penicillin-streptomycin solution. All cells were grown at 310 K in a humidified incubator under a 5% CO₂ atmosphere.

Viability assay (MTT assay). After plating 5000 A549 cells per well in 96-well plates, the cells were preincubated in drug-free media at 310 K for 24 h or 72 h before adding different concentrations of the compounds to be tested. In order to prepare the stock solution of the drug, the solid complex was dissolved in DMSO. This stock was further diluted using cell culture medium until working concentrations were achieved. The drug exposure period was 24 h or 72 h. Subsequently, 15 μL of 5 mg mL^{-1} MTT solution was added to form a purple formazan. Afterwards, 100 μL of dimethyl sulfoxide (DMSO) was transferred into each well to dissolve the purple formazan, and results were measured using a microplate reader (DNM-9606, Perlong Medical, Beijing, China) at an absorbance of 570 nm. Each well was triplicated and each experiment repeated at least three times. IC₅₀ values quoted are mean \pm SEM.

Localization Experiments. Localization of complex (10 μM) with mitochondria or lysosome were examined by means of MTDR (MitoTracker Deep Red) (Molecular Probes), a mitochondria-specific dye and LTDR (LysoTracker Deep Red), a lysosome-specific dye. Briefly, A549 cells were seeded into 6-well plates (Greiner, Germany) for confocal microscopy. After cultured overnight, a 1 mM complex stock solution made in DMSO was diluted to 10 μM working concentration in cell medium (DMEM, 5% FCS). Staining of mitochondria/lysosome was accomplished by adding a 75 nM/100 nM final concentration of MTDR/LTDR to the culture medium for the last 30 min of complex incubation. The medium was removed and washed three times with ice-cold PBS, and then viewed immediately under a confocal microscope (Zeiss LSM880 NLO). The excitation and emission bands of each compound were selected as follows for complex: $\lambda_{\text{ex}} = 488 \text{ nm}$; $\lambda_{\text{em}} = 550 \pm 20 \text{ nm}$. MTDR: $\lambda_{\text{ex}} = 644 \text{ nm}$; $\lambda_{\text{em}} = 660 \pm 20 \text{ nm}$. LTDR: $\lambda_{\text{ex}} = 594 \text{ nm}$; $\lambda_{\text{em}} = 650 \pm 20 \text{ nm}$.

Inductively coupled plasma mass spectrometry (ICP-MS). A549 cells were seeded in 90 mm dishes for 24 h (three dishes were prepared per compound tested). The media was removed and replaced with fresh media containing the tested complex (5 μM) for 24 h. After the removal of the culture media and rinse with 1 mL of PBS buffer (1X), the cells were treated with 500 μL of 0.25% trypsin and centrifuged at 1000 rpm. The cells were counted, one half of the cells were centrifuged, quickly washed with PBS, and stored at 253 K for determination of total cell accumulation of ruthenium. Another half of the samples was used for cytosol and nucleus, using a nuclear and cytoplasmic protein extraction kit (Shanghai Sangon Biological Engineering Technology & Services Co. Ltd.). The samples were nitrolysis with concentrated HNO₃ at 95 $^{\circ}\text{C}$ for 2 h, H₂O₂ at 95 $^{\circ}\text{C}$ for 1.5 h and concentrated HCl at 37 $^{\circ}\text{C}$ for 0.5 h. Finally, the solution was diluted to 2 mL with MQ water and the Pt content was measured by the inductively coupled plasma mass spectrometer (ICP-MS; VG Elemental).

Cellular Uptake. A549 cells were seeded in 6-well plates for 24 h and preincubated with CCCP (50 μ M) or chloroquine (50 μ M) for 1 h. The medium was removed and the cells were then incubated with complex (10 μ M) for 1 h. To investigate the impact of temperature on cellular uptake, the cells were incubated at 4 $^{\circ}$ C or 37 $^{\circ}$ C for 1 h. In each case, the cells were washed three times with ice-cold PBS and visualize by confocal microscopy (Zeiss LSM880NLO) immediately. $\lambda_{\text{ex}}= 488 \text{ nm}$, $\lambda_{\text{em}}= 550 \pm 20 \text{ nm}$.

Induction of Apoptosis. Flow cytometry analysis of apoptotic populations of A549 cells caused by exposure to metal complexes was carried out using the Annexin V-FITC Apoptosis Detection Kit (Beyotime Institute of Biotechnology, China) according to the supplier's instructions. Briefly, A549 cells ($1.5 \times 10^6/2 \text{ mL}$ per well) were seeded in a six-well plate. Cells were preincubated in drug-free media at 310 K for 24 h, after which drugs were added at concentrations of $1 \times \text{IC}_{50}$, $2 \times \text{IC}_{50}$ and $3 \times \text{IC}_{50}$. After 24 h of drug exposure, cells were collected, washed once with PBS, and resuspended in 195 μ L of annexin V-FITC binding buffer which was then added to 5 μ L of annexin V-FITC and 10 μ L of PI, and then incubated at room temperature in the dark for 15 min. Subsequently, the buffer placed in an ice bath in the dark. The samples were analyzed by a flow cytometer (ACEA NovoCyte, Hangzhou, China).

Cell Cycle Analysis. A549 cells at 1.5×10^6 per well were seeded in a six-well plate. Cells were preincubated in drug-free media at 310 K for 24 h, after which drugs were added at concentrations of $0.25 \times \text{IC}_{50}$, $0.5 \times \text{IC}_{50}$ and IC_{50} . After 24 h of drug exposure, supernatants were removed by suction and cells were washed with PBS. Finally, cells were harvested using trypsin-EDTA and fixed for 24 h using cold 70 % ethanol. DNA staining was achieved by resuspending the cell pellets in PBS containing propidium iodide (PI) and RNase. Cell pellets were washed and resuspended in PBS before being analyzed in a flow cytometer (ACEA NovoCyte, Hangzhou, China) using excitation of DNA-bound PI at 488 nm, with emission at 585 nm. Data were processed using NovoExpress™ software. The cell cycle distribution is shown as the percentage of cells containing G₀/G₁, S G₂/M and Sub-G₁ phase DNA as identified by propidium iodide staining.

ROS Determination. Flow cytometry analysis of ROS generation in A549 cells caused by exposure to metal complexes was carried out using the Reactive Oxygen Species Assay Kit (Beyotime Institute of Biotechnology, Shanghai, China) according to the supplier's instructions. Briefly, 1.5×10^6 A549 cells per well were seeded in a six-well plate. Cells were preincubated in drug-free media at 310 K for 24 h in a 5% CO₂ humidified atmosphere, and then drugs were added at concentrations of $0.25 \times \text{IC}_{50}$ and $0.5 \times \text{IC}_{50}$. After 24 h of drug exposure, cells were washed twice with PBS and then incubated with the DCFH-DA probe (10 μ M) at 37 $^{\circ}$ C for 30 min, and then washed triple immediately with PBS. The fluorescence intensity was analyzed by flow cytometry (ACEA NovoCyte, Hangzhou, China). Data were processed using NovoExpress™ software. At all times, samples were kept under dark conditions to avoid light-induced ROS production.

Mitochondrial Membrane Assay. Analysis of the changes of mitochondrial potential in cells after exposure to metal complex was carried out using the Mitochondrial membrane potential

assay kit with JC-1 (Beyotime Institute of Biotechnology, Shanghai, China) according to the manufacturer's instructions. Briefly, 1.5×10^6 A549 cancer cells were seeded in six-well plates left to incubate for 24 h in drug-free medium at 310 K in a humidified atmosphere. Drug solutions, at concentrations of $0.25 \times IC_{50}$, $0.5 \times IC_{50}$, $1 \times IC_{50}$ and $2 \times IC_{50}$ of complex against A549 cancer cells, were added in triplicate, and the cells were left to incubate for a further 24 h under similar conditions. Supernatants were removed by suction, and each well was washed with PBS before detaching the cells using trypsin-EDTA. Staining of the samples was done in flow cytometry tubes protected from light, incubating for 30 min at ambient temperature. The samples were immediately analyzed by a flow cytometer (ACEA NovoCyte, Hangzhou, China). For positive controls, the cells were exposed to carbonyl cyanide 3-chlorophenylhydrazone, CCCP (5 μ M), for 20 min. Data were processed using NovoExpress™ software.

ASSOCIATED CONTENT

The Supporting Information is available free of charge on the Publications website at DOI: xxx xxx xxx.

Experimental Section, Fig. S1- Fig. S5. Table S1 – Table S3 (PDF).

AUTHOR INFORMATION

Corresponding author.

Email: liuzheqd@163.com

ORCID

Zhe Liu: 0000-0001-5796-4335

Author Contributions

All authors have given approval to the final version of the manuscript.

Conflicts of interest

There are no conflicts of interest to declare.

ACKNOWLEDGMENTS

We thank the National Natural Science Foundation of China (GrantNo.21671118) and the Taishan Scholars Program for support.

References

1. C. A. Puckett, R. J. Ernst and J. K. Barton, *Dalton Trans.*, 2010, **39**, 1159-1170.
2. N. Muhammad and Z. Guo, *Curr. Opin. Chem. Biol.*, 2014, **19**, 144-153.
3. J. X. Liang, H. J. Zhong, G. Yang, K. Vellaisamy, D. L. Ma and C. H. Leung, *J. Inorg. Biochem.*, 2017, **177**, 276-286.
4. C.-H. Leung, S. Lin, H.-J. Zhong and D.-L. Ma, *Chem. Sci.*, 2015, **6**, 871-884.
5. T. W. Hambley, *Dalton Trans.*, 2007, 4929-4937.
6. S. M. Emam, I. E. T. El Sayed and N. Nassar, *Spectrochim. Acta. A Mol. Biomol. Spectrosc.*, 2015, **138**, 942-953.
7. M. A. Malik, O. A. Dar, P. Gull, M. Y. Wani and A. A. Hashmi, *MedChemComm*, 2018, **9**, 409-436.
8. Y. Wang, H. Wang, H. Li and H. Sun, A. Mudipalli and J. T. Zelikoff, Springer International Publishing, Cham, 2017, pp. 199-222.
9. Q. Cao, Y. Li, E. Freisinger, P. Z. Qin, R. K. O. Sigel and Z. W. Mao, *Inorg. Chem. Front.*, 2017, **4**,

- 10-32.
10. R. Guan, Y. Chen, L. Zeng, T. W. Rees, C. Jin, J. Huang, Z. S. Chen, L. Ji and H. Chao, *Chem. Sci.*, 2018, **9**, 5183-5190.
 11. Y. Huang, W. Huang, L. Chan, B. Zhou and T. Chen, *Biomaterials*, 2016, **103**, 183-196.
 12. M. D. Hall and T. W. Hambley, *Coord. Chem. Rev.*, 2002, **232**, 49-67.
 13. R. A. Alderden, M. D. Hall and T. W. Hambley, *J. Chem. Educ.*, 2006, **83**, 728.
 14. A. V. Klein and T. W. Hambley, *Chem. Rev.*, 2009, **109**, 4911-4920.
 15. R. E. Aird, J. Cummings, A. A. Ritchie, M. Muir, R. E. Morris, H. Chen, P. J. Sadler and D. I. Jodrell, *Br. J. Cancer*, 2002, **86**, 1652.
 16. C. G. Hartinger and P. J. Dyson, *Chem. Soc. Rev.*, 2009, **38**, 391-401.
 17. J. Li, L. Guo, Z. Tian, M. Tian, S. Zhang, K. Xu, Y. Qian and Z. Liu, *Dalton Trans.*, 2017, **46**, 15520-15534.
 18. J. Li, M. Tian, Z. Tian, S. Zhang, C. Yan, C. Shao and Z. Liu, *Inorg. Chem.*, 2018, **57**, 1705-1716.
 19. M. Tian, J. Li, S. Zhang, L. Guo, X. He, D. Kong, H. Zhang and Z. Liu, *Chem. Commun.*, 2017, **53**, 12810-12813.
 20. Z. Xu, D. Kong, X. He, L. Guo, X. Ge, X. Liu, H. Zhang, J. Li, Y. Yang and Z. Liu, *Inorg. Chem. Front.*, 2018, 2100-2105.
 21. L. Zeng, P. Gupta, Y. Chen, E. Wang, L. Ji, H. Chao and Z. S. Chen, *Chem. Soc. Rev.*, 2017, **46**, 5771-5804.
 22. L. Biancalana, L. K. Batchelor, T. Funaioli, S. Zacchini, M. Bortoluzzi, G. Pampaloni, P. J. Dyson and F. Marchetti, *Inorg. Chem.*, 2018, **57**, 6669-6685.
 23. A.-d. C. Silvia, C. A. L., L.-G. Fernando and S. Luca, *Angew. Chem.*, 2018, **130**, 3197-3201.
 24. F. Martínez-Peña, S. Infante-Tadeo, A. Habtemariam and A. M. Pizarro, *Inorg. Chem.*, 2018, **57**, 5657-5668.
 25. S. Thota, D. A. Rodrigues, D. C. Crans and E. J. Barreiro, *J. Med. Chem.*, 2018, **61**, 5805-5821.
 26. G. Sava, S. Pacor, G. Mestroni and E. Alessio, *Clin. Exp. Metastasis*, 1992, **10**, 273-280.
 27. P. Costantini, E. Jacotot, D. Decaudin and G. Kroemer, *J. Natl. Cancer Inst.*, 2000, **92**, 1042-1053.
 28. L. He, Y. Li, C. P. Tan, R. R. Ye, M. H. Chen, J. J. Cao, L. N. Ji and Z. W. Mao, *Chem. Sci.*, 2015, **6**, 5409-5418.
 29. J. Li, L. Guo, Z. Tian, S. Zhang, Z. Xu, Y. Han, R. Li, Y. Li and Z. Liu, *Inorg. Chem.*, 2018, **57**, 13552-13563.
 30. J. Li, Z. Tian, Z. Xu, S. Zhang, Y. Feng, L. Zhang and Z. Liu, *Dalton Trans.*, 2018, **47**, 15772-15782.
 31. W. Ma, Z. Tian, S. Zhang, X. He, J. Li, X. Xia, X. Chen and Z. Liu, *Inorg. Chem. Front.*, 2018, **5**, 2587-2597.
 32. Z. Tian, J. Li, S. Zhang, Z. Xu, Y. Yang, D. Kong, H. Zhang, X. Ge, J. Zhang and Z. Liu, *Inorg. Chem.*, 2018, **57**, 10498-10502.
 33. X. Jia, H. Liu, Y. Hu, Q. Dai, J. Bi, C. Bai and X. Zhang, *Chinese J. Catal.*, 2013, **34**, 1560-1569.
 34. F. K. Cheung, C. Lin, F. Minissi, A. L. Crivillé, M. A. Graham, D. J. Fox and M. Wills, *Org. Lett.*, 2007, **9**, 4659-4662.
 35. F. X. Wang, M. H. Chen, Y. N. Lin, H. Zhang, C. P. Tan, L. N. Ji and Z. W. Mao, *ACS Appl. Mater. Inter.*, 2017, **9**, 42471-42481.
 36. J. J. Soldevila-Barreda, I. Romero-Canelón, A. Habtemariam and P. J. Sadler, *Nat. Commun.*,

- 2015, **6**, 6582-6590.
37. L. Zhe, R. C. Isolda, Q. Bushra, H. J. M., H. Abraha, B. N. P. E., P. A. M., C. G. J. and S. P. J., *Angew. Chem.*, 2014, **126**, 4022-4027.
38. W. Yang, L. Shenglin, Z. Chi, L. Xingyun, L. Tao, J. Zhongyong, L. Dengqun, T. Xu, L. Lei, W. Yu, C. Zelin, L. Yunsheng, Y. Fan, G. Yibo and S. Chunmeng, *Advanced Materials*, 2018, **0**, 1800475.
39. M. T. Gyparaki and A. G. Papavassiliou, *Trends Mol. Med.*, 2014, **20**, 239-241.
40. D. Y. Zhang, Y. Zheng, C. P. Tan, J. H. Sun, W. Zhang, L. N. Ji and Z. W. Mao, *ACS Appl. Mater. Inter.*, 2017, **9**, 6761-6771.
41. Y. Li, C.-P. Tan, W. Zhang, L. He, L.-N. Ji and Z.-W. Mao, *Biomaterials*, 2015, **39**, 95-104.
42. J. Ji, X. Li, T. Wu and F. Feng, *Chem. Sci.*, 2018, **9**, 5816-5821.